J Mater Sci (2008) 43:2411–2417
DOI 10.1007/s10853-007-2110-z

UV Shielding performance enhancement of CaO doped ceria by coupling with plate-like $K_{0.8}Li_{0.27}Ti_{1.73}O_4$

Ahmed Mohamed El-Toni · Shu Yin · Tsugio Sato

Received: 7 November 2006 / Accepted: 13 August 2007 / Published online: 22 November 2007

Abstract CaO-doped ceria is of potential interest as an ultraviolet (UV) radiation blocking material in personal care products because of its excellent UV light absorption property and low catalytic ability for the oxidation of organic materials. The performance of CaO-doped ceria needs more enhancements through further control of its oxidation catalytic activity and improvement of its covering ability. The oxidation catalytic activity of CaO-doped ceria may be further reduced by coating with amorphous silica. Generally, CaO-doped ceria do not provide a good coverage for human skin because of the agglomeration of the nanoparticles. The plate-like particles can be used to enhance the covering ability of CaO-doped ceria. Therefore, CaO-doped ceria ($Ce_{0.8}Ca_{0.2}O_{1.8}$)/plate-like potassium lithium titanate ($K_{0.8}Li_{0.27}Ti_{1.73}O_4$) nanocomposite was synthesized followed by subsequent silica coating.

Introduction

Fine powder of ceria (CeO_2) has characteristics ideal for use as a broad-spectrum inorganic sunscreen in personal care products: It is quite transparent to visible light, but has excellent ultraviolet absorption ability, and appears natural on the skin without imparting an excessively pale white look, since the value of the refractive index of ceria (n = 2.05) is lower than that of rutile (n = 2.72), anatase (n = 2.5), and zinc oxide (n = 2.2). Fine particles of titania and zinc oxide are effective inorganic sunscreens widely used in personal care products, but their high refractive indices can make the skin look unnaturally white. In addition, their high photocatalytic activity facilitates the generation of reactive oxygen species, raising safety concerns [1]. Many studies have reported about synthesis of nano-sized particles of ceria with various purposes [2–8]. However, because of its high catalytic ability for the oxidation of organic materials, it has been seldom commercially used as sunscreen. The catalytic ability of ceria would be related with oxygen release and absorption equilibrium reaction shown by Eq. (1).

$$CeO_2 \rightleftarrows Ce^{4+}_{1-X}Ce^{3+}_{X}O_{2-X/2}V_{oX/2} + X/4O_2 \quad (V_o\text{: oxygen defect, } 0<x<1) \tag{1}$$

Yabe et al. [9] suggested that the evolution of oxygen from ceria would be depressed by doping with metal ion possessing larger ionic size to stabilize fluorite structure and/or lower valence metal ion to shift the equilibrium of Eq. (1) to the left hand side by forming oxygen defect. Actually, doping with calcium ion, which has larger ionic size and lower valence, resulted in reasonable depression of catalytic ability of ceria nanoparticles [10], however, the oxidation catalytic ability of CaO-doped ceria was still high. A number of studies have been reported on coating of different kinds of fine particles with silica [11–21]. The oxidation catalytic ability of CaO-doped ceria could be greatly depressed by forming a film of silica on the surface by the sol–gel technique [22]. Generally, nanoparticles of CaO-doped ceria do not provide a good coverage for human skin because of the agglomeration of the particles. The plate-like particles are required to enhance the covering ability of CaO-doped ceria. Potassium lithium titanate materials consist of sheets arranged parallel to each other. The interactions between the sheets are relatively weak, allowing potassium lithium titanate materials to be peeled or split into flat sheets. The weak interactions between the

A. M. El-Toni (✉) · S. Yin · T. Sato
Institute of Multidisciplinary Research for Advanced Materials, Tohoku University, Sendai 980-8577, Japan
e-mail: el-toni@mail.tagen.tohoku.ac.jp

plate-like materials sheets allow the sheets to slide past each other in some cases, resulting in the slippery feel and better distribution on human skin. Consequently, upon coupling of CaO-doped ceria with plate-like materials, two advantages will be attained. First, soft and nice feeling will be acquired for agglomerated CaO-doped ceria. Second, better distribution with improving coverage ability of CaO-doped ceria which will finally enhance the UV-shielding property of CaO-doped ceria. Subsequent silica coating was performed for CaO-doped ceria/plate-like potassium lithium titanate nanocomposite to control catalytic activity of CaO-doped ceria. In this work, CaO-doped ceria/plate-like potassium lithium titanate nanocomposite was prepared by soft chemical method followed by silica coating via sol–gel technique. Silica-coated CaO-doped ceria/plate-like potassium lithium titanate nanocomposite was characterized by X-ray diffraction, SEM, TEM, XPS, and FT-IR.

Experimental

Synthesis

Synthesis of $K_{0.8}Li_{0.27}Ti_{1.73}O_4$

Syntheses of lepidocrocite-related titanate were conducted by flux [23] and calcination methods [24]. The typical procedures to prepare potassium lithium titanate by flux melting method were as follows. The powders of K_2CO_3, Li_2CO_3, and TiO_2 (anatase form) were mixed intimately in molar ratio of 3:1:13 (nominal composition: $K_{0.8}Li_{0.266}Ti_{1.734}O_4$) and the mixture was placed in a Pt crucible and heated at 800 °C for 30 min to be decarbonated. After cooling, the raw material was ground along with K_2MoO_4 (flux) with different weight ratios (50:50, 33:67, and 20:80), put in a Pt crucible and then heated up to 1,000°C at a heating rate of 200 °C h^{-1} then the temperature was fixed at 1,000 °C for 120 min. After that the temperature was decreased to 800 °C at a rate of 50 °C h^{-1} and then to room temperature naturally. To clarify the optimum reaction conditions, the effects of the reaction temperature, weight ratio of raw material to flux, reaction time, and lithium content on the particle morphology were investigated. All experimental products were washed with boiling water to remove the K_2MoO_4 flux and dried at 80 °C.

Synthesis of CaO doped ceria/potassium lithium titanate nanocomposite

CaO-doped ceria/potassium lithium titanate (70:30 wt%) was synthesized using the soft solution chemical route as follows [22]. After putting potassium lithium titanate particles in deionized water at 40 °C, appropriate quantities of 3 M NaOH aqueous solution and 0.8 M $CeCl_3$–0.2 M $CaCl_2$ mixed aqueous solution were simultaneously dropped, where the solution was stirred and pH was kept at 12 through the reaction. Then, the desired amount of 2 M H_2O_2 solution was added and pH was also kept at 12. The chemical reactions can be expressed by Eqs. (2) and (3).

$$0.8\ CeCl_3 + 0.2\ CaCl_2 + 2.8\ NaOH \rightarrow Ce_{0.8}\ Ca_{0.2}(OH)_{2.8} + 2.8\ NaCl \quad (2)$$

$$Ce_{0.8}Ca_{0.2}(OH)_{2.8} + 0.4H_2O_2 \rightarrow Ce_{0.8}Ca_{0.2}O_{1.8} + 1.8H_2O \quad (3)$$

The slurry was filtrated and washed with water and methanol. The precipitate was fired at 700 °C for 1 h to obtain potassium lithium titanate coated with white CaO-doped ceria nanoparticles.

Silica coating of CaO-doped ceria/potassium lithium titanate nanocomposite

CaO-doped ceria/potassium lithium titanate nanocomposite was coated with 5 wt% silica via sol–gel technique as follows [22]. After dispersing CaO-doped ceria/potassium lithium titanate nanocomposite powder in TEOS/ethanol mixed solution, predetermined amount of water and 29 wt% ammonia aqueous solution were stepwise added and then the solution was stirred for a desired time at 40 °C. The molar ratio of TEOS:ethanol:water:ammonia was 1:100:400:20.

Characterizations

The crystalline phase was determined by X-ray powder diffraction analysis (SHIMADZU, XD-01) with CuKα radiation. The catalytic ability for oxidation of organic material was determined by a conductometric determination method (Rancimat method) [25] using castor oil of cosmetic grade as oxidized material. The sample powder (1 g) was mixed with castor oil (10 g) and set at 120 °C with bubbling 500 cm^3 min^{-1} of air, where the air was introduced into deionized water. The catalytic ability was determined by measuring the increase in the electric conductivity of deionized water by trapping the volatile molecules coming from the oxidation of castor oil on heating.

The UV-shielding ability of non-coated and silica coated samples were evaluated by measuring the transmittance spectra of thin films uniformly dispersed the sample powders with an UV–Vis spectrophotometer (SHIMADZU, UV-2450), where 2 g of the sample, 4 g of nitrocellulose

of industrial grade, 10 g of ethyl acetate, and 9 g of butyl acetate were mixed uniformly using the paint shaker and 100 g of zirconia ball with 2.7 mm in diameter for 40 h. The dispersion mixture was applied onto a quartz glass plate with an applicator. Thickness of the film was 12.5 μm. FTIR measurements were conducted using FTS 7000 series, DIGILIB. The particle morphology was evaluated by a transmission electron microscope (JEM-2000 EX). A scanning electron microscope (Hitachi S 4100) was used to study the surface morphology.

XPS spectra were measured at room temperature by X-ray electron spectrometer (Perkin Elmer PHI 5600) and O1s spectra was collected for non-coated and silica coated samples.

The low-level luminous intensity of chemiluminescence of singlet oxygen ($^1O_2$) was directly measured with a multichemiluminescence spectrometer (MLA-GOLDS-S; Tohoku Electric Ind.). Approximately 1 g of the sample powder was placed into a stainless steel cell (50 mm in diameter and 10 mm in depth) covered with a quartz cell. The test sample was irradiated in air with UV rays of 254 nm for 5 s at room temperature. Chemiluminescence intensity was measured 5 s later for 100 s, where a red filter which can transmit only a light of wavelength greater than 600 nm was placed between the cuvette and the photomultiplier to cut off the emission attributed to carbonyl compounds.

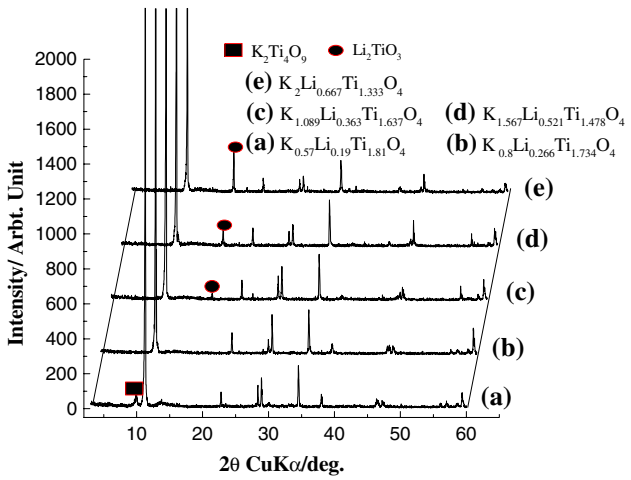

Fig. 1 Powder X-ray diffraction patterns of the samples formed with various lithium contents and a raw material to flux weight ratio of 50:50 at 1,000°C for 120 min and cooling rate of 50 °C h^{-1}. Nominal Li content x in $K_{3x}Ti_{2-x}Li_xO_4$: (**a**) 0.19, (**b**) 0.266, (**c**) 0.363, (**d**) 0.521, and (**e**) 0.667

Result and discussion

Synthesis of $K_{0.8}Li_{0.27}Ti_{1.73}O_4$: effect of Li content

The powder X-ray diffraction patterns of potassium lithium titanate at different nominal Li contents ($K_{3x}Ti_{2-x}Li_xO_4$) are shown in Fig. 1. It can be observed that at Li content x = 0.19, potassium tetratitanate ($K_2Ti_4O_9$) was formed in addition to lepidocrocite-related titanate. Increasing Li content to x = 0.266 resulted in the formation of single phase lepidocrocite-related titanate. The chemical composition may be described as $K_{0.8}Li_{0.266}Ti_{1.734}O_4$. On the other hand, Li_2TiO_3 appeared together with the lepidocrocite-related titanate at nominal Li contents x ≥ 0.363.

SEM micrographs for different Li contents are shown in Fig. 2. SEM micrographs (Fig. 2a) for x = 0.19 shows the formation of plate-like titanate particle along with needle-like particles which was identified as potassium tetratitanate ($K_2Ti_4O_9$). Increasing Li content thereafter do not affect formation of plate-like titanate but resulted in decrease of particle size (Fig. 2 b and c).

Optimization of synthesis parameters indicated that the lower lithium content resulted in the formation of needle-like potassium tetratitanate while higher Li content (above x ≥ 0.363) led to the formation of plate-like titanate along with lithium titanate. The flux (K_2MoO_4) helps in enhancement of the crystallinity and particle size of potassium lithium titanate. Decreasing reaction temperature and time resulted in decreasing the particle size. The optimum synthesis parameters to obtain plate-like potassium lithium titanate with ca. 15–20 μm are determined as flux: raw materials weight ratio of 50:50, reaction temperature of 950 °C, reaction time of 120 min, and x in $K_{3x}Ti_{2-x}Li_xO_4$ of 0.266.

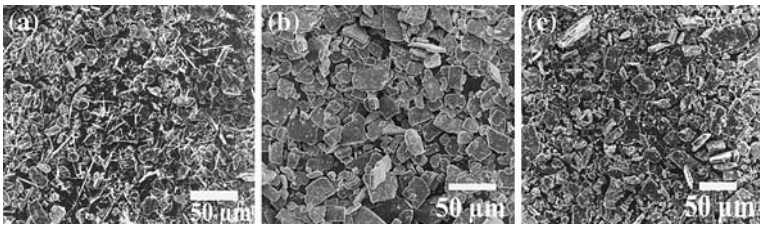

Fig. 2 SEM micrographs of the samples formed with a raw material to flux weight ratio of 50:50 at 1,000 °C for 120 min and cooling rate of 50 °C h^{-1} with the nominal Li content x in $K_{3x}Ti_{2-x}Li_xO_4$ of (**a**) 0.19, (**b**) 0.266, and (**c**) 0.521

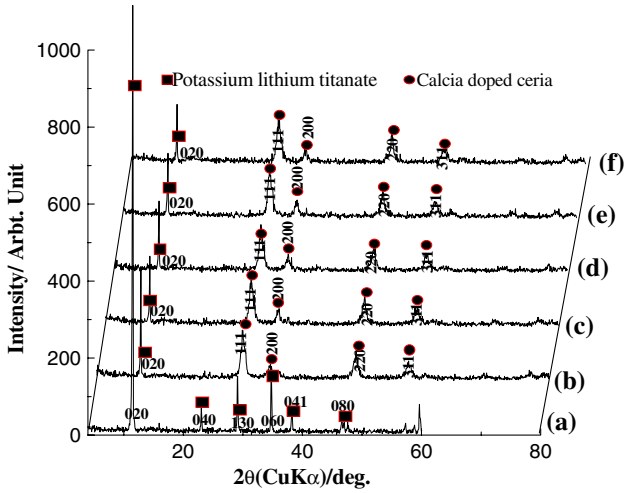

Fig. 3 Powder X-ray diffraction patterns of (**a**) potassium lithium titanate (**b**) CaO-doped ceria/potassium lithium titanate, 5% silica coated CaO-doped ceria/potassium lithium titanate after coating times of (**c**) 45, (**d**) 90, (**e**) 180, and (**f**) 360 min

Coating and photochemical properties of $Ce_{0.8}Ca_{0.2}O_{1.8}/K_{0.8}Li_{0.27}Ti_{1.73}O_4$ nanocomposite

The powder X-ray diffraction patterns of CaO-doped ceria/potassium lithium titanate before and after coating with silica for different coating times are shown in Fig. 3. All peaks could be attributed to ceria with fluorite structure and lepidocrocite-type layered titanate. There was no noticeable effect of silica coating time on peak position and peak intensity.

SEM micrographs for potassium lithium titanate and CaO-doped ceria/potassium lithium titanate nanocomposite are shown in Fig. 4. It can be seen that potassium lithium titanate possesses regular plate-like structure with particle size range of 15–20 μm. (Fig. 4a). It can be observed that CaO-doped ceria nanoparticles were precipitated on the surface of plate-like titanate particles (Fig. 4b).

Figure 5a shows that the surface of potassium lithium titanate particle is covered with CaO-doped ceria nanoparticles. Higher magnification of transmission electron micrograph of 5 wt% silica coated CaO-doped ceria/mica (Fig. 5b) clearly shows the formation of silica shell ca. 2 nm thickness on CaO-doped ceria nanoparticles.

Figure 6 shows XPS spectra of (a) silica, (b) plate-like potassium lithium titanate, (c) CaO-doped ceria, (d) CaO-doped ceria/plate-like potassium lithium titanate, CaO-doped ceria/plate-like potassium lithium titanate coated with 5 wt% silica for (e) 180 min. Figure 6a shows characteristic peaks of silica at 103.8, 160 of Si2p and Si2s, respectively. XPS spectrum of (d) CaO-doped ceria/plate-like potassium lithium titanate is almost identical with that of (c) CaO-doped ceria, indicating no peak corresponding to potassium lithium titanate shown in Fig. 6b. Since XPS is a rather surface sensitive technique (the sampling depth here is below ~4 nm, depending on electro kinetic energy), the spectrum reveals chemical state of outer layer of the particle. Accordingly XPS spectrum of CaO-doped ceria/plate-like potassium lithium titanate particles (Fig. 6d) shows only the peaks characteristic for CaO-doped ceria at 888.5 and 882.3 eV corresponded to

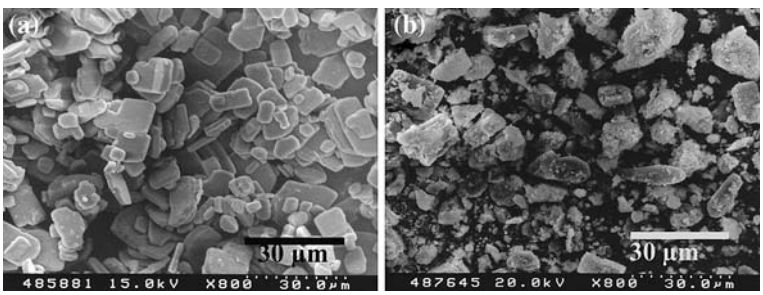

Fig. 4 SEM micrographs for (**a**) potassium lithium titanate, (**b**) CaO-doped ceria/potassium lithium titanate

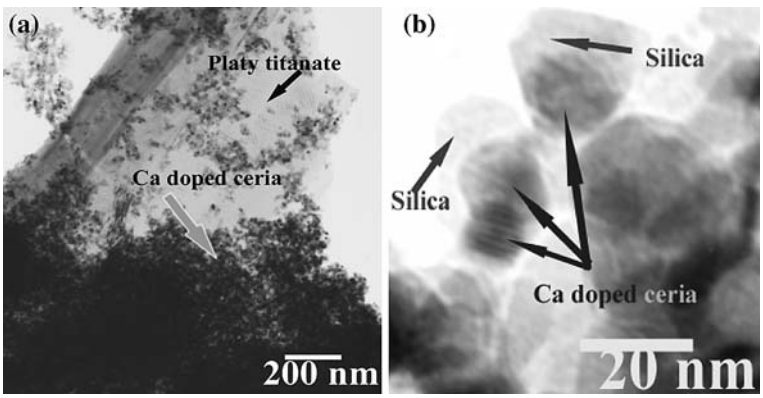

Fig. 5 TEM micrographs of (**a**) potassium lithium titanate, (**b**) CaO-doped ceria/potassium lithium titanate, (**c**) 5 wt% silica-coated CaO-doped ceria/potassium lithium titanate after coating time of 180 min at higher magnification

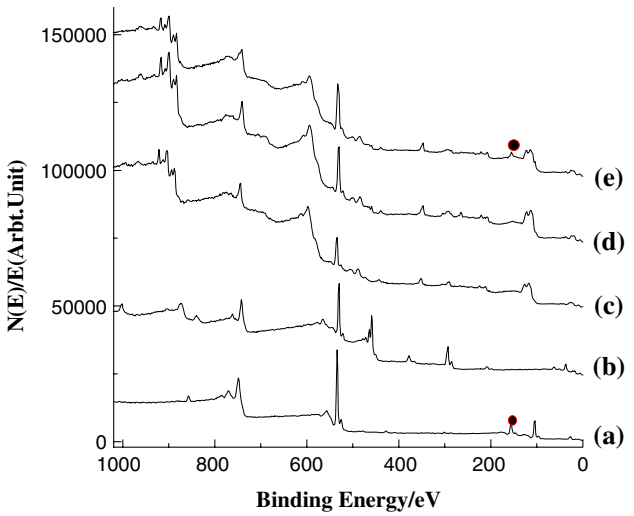

Fig. 6 XPS spectra of (**a**) silica, (**b**) potassium lithium titanate, (**c**) CaO-doped ceria, (**d**) CaO-doped ceria/potassium lithium titanate, CaO-doped ceria/potassium lithium titanate coated with 5 wt% silica for (**e**) 180 min

Ce^{4+} and at 346.4 eV assigned to Ca2p. XPS spectra of 5 wt% silica coated CaO-doped ceria/plate-like potassium lithium titanate at coating time of 180 min, (Fig. 6 e), show the characteristic peaks of CaO-doped ceria in addition to that of silica at 160 eV of Si2s which indicates coating of CaO-doped ceria with thin layer of silica.

Figure 7 shows XPS O1s core level spectra of (d) non-coated and (e) silica-coated CaO-doped ceria/plate-like potassium lithium titanate together with those of (a) CaO-doped ceria, (b) silica, and (c) plate-like potassium lithium titanate. It is clear that several types of lattice oxygen are present. For CaO-doped ceria (Fig. 7a), a large one at 528.5 eV was attributed to lattice oxygen ion in CaO-doped ceria, and a smaller one at 531 eV was attributed to adsorbed oxygen. Fig. 7b shows XPS O1s core level spectra of silica at 532.8 eV, while that of potassium lithium titanate appeared at 529.5 eV (Fig. 7c). Similarity of O1s spectra of CaO-doped ceria/ potassium lithium titanate and that of CaO-doped ceria (Fig. 7a, d) without a notice of any shift of binding energy, suggests that CaO-doped ceria physically covers the potassium lithium titanate surface and there is no chemical linkage was developed at the interface. On the other hand, XPS O1s core level spectra of 5 wt% silica-coated CaO-doped ceria/potassium lithium titanate at coating times of 180 min (Fig. 7e) show peaks at 529.2 and 532.8. eV attributed to CaO-doped ceria and silica, indicating the coating of CaO-doped ceria with thin silica layer. It can be deduced that the 529.2 eV peak of O 1s in silica-coated CaO-doped ceria resulted from a chemical shift of 528.5 eV peak of O 1s in pure CaO-doped ceria. In the silica-coated CaO-doped ceria powder, it is inferred that silica is combined with CaO-doped ceria to form a Ce–O–Si bond. Since the electronegativity of Si is greater than that of Ce, O 1s peak for CaO-doped ceria has a chemical shift of +0.7 eV.

FT-IR measurement was conducted for non-coated and silica-coated CaO-doped ceria/potassium lithium titanate as shown in Fig. 8. Spectrum of CaO-doped ceria shows weak peak in range of 750–800 cm^{-1} and strong one at 1,400 cm^{-1} which is characteristic of different metal–oxygen bonds (Fig. 8a). Characteristic peaks for plate-like potassium lithium titanate appeared as medium one at 800 cm^{-1} then a broad peak from 1,800–3,500 cm^{-1}.

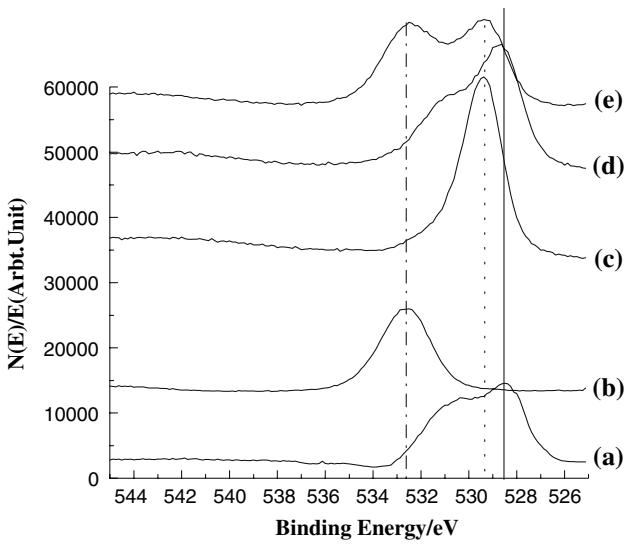

Fig. 7 XPS spectra of (**a**) CaO-doped ceria, (**b**) silica, (**c**) potassium lithium titanate, (**d**) CaO-doped ceria/potassium lithium titanate, CaO-doped ceria/potassium lithium titanate coated with 5 wt% silica for (**e**) 180 min in the O1s energy range

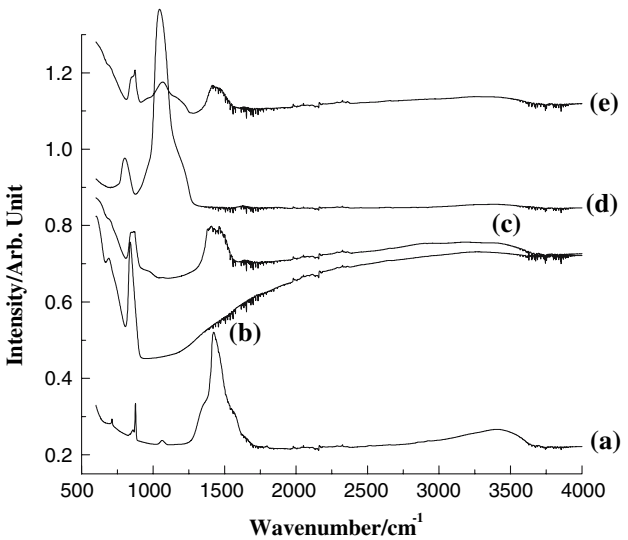

Fig. 8 FTIR spectra (**a**) CaO-doped ceria, (**d**) silica, (**b**) potassium lithium titanate, (**c**) CaO-doped ceria/potassium lithium titanate, CaO-doped ceria/potassium lithium titanate coated with 5 wt% silica for (**e**) 180 min

Non-coated CaO-doped ceria/potassium lithium titanate (Fig. 8c) shows medium peak at 800 cm^{-1} which is characteristic for plate-like potassium lithium titanate and strong peak being characteristic for CaO-doped ceria at 1,400 cm^{-1}, revealing the formation of nanocomposite between plate-like potassium lithium titanate and CaO-doped ceria. After 5 wt% silica coating for 180 min (Fig. 8 e), the characteristic peak for silica appeared as medium one at 1,100 cm^{-1}, indicating coating of CaO-doped ceria/potassium lithium titanate with silica.

Figure 9 shows the results of the oxidation catalytic activity evaluation by Rancimat method for non-coated and 5wt % silica-coated CaO-doped ceria/potassium lithium titanate. As expected, the catalytic ability of CaO-doped ceria/potassium lithium titanate for air oxidation of castor oil at 120 °C decreased substantially by silica coating. It can be seen that the oxidation catalytic activity of CaO-doped ceria/potassium lithium titanate nanocomposite is lower than CaO-doped ceria probably due to the decrease of CaO-doped ceria content by 30 wt%. Increasing silica coating time helps to delay the oxidation of castor oil by CaO-doped ceria/potassium lithium titanate and 180 min of coating time seems to be optimum.

It is well-known that active oxygen species such as $\bullet O_2^-$, •OOH, •OH and $^1O_2$ (singlet oxygen) are formed by the band gap excitation of semiconductors in air and play important role for the photocatalytic reactions. Singlet oxygen has so-called dimole emission (Eq. 4) and monomole emission (Eq. 5) [26].

$$^1O_2 + {}^1O_2 \rightarrow 2\,{}^3O_2 + h\nu \ (634 \text{ and } 703\ \text{nm}) \quad (4)$$

$$^1O_2 \rightarrow {}^3O_2 + h\nu \ (1270\ \text{nm}) \quad (5)$$

By the chemiluminescence assay, it was indicated that the amounts of $^1O_2$ generation on the surface of non-coated and silica-coated CaO-doped ceria/potassium lithium titanate were much lower than that on zinc oxide and titania (Fig. 10). Also it can be notice that silica-coated CaO-doped ceria/plate-like potassium lithium titanate showed similar low emission intensity to CaO-doped ceria. These results suggested that the photocatalytic activity of CaO-doped ceria and potassium lithium titanate are much lower than that of zinc oxide and titanate which is the great advantage of these materials for the cosmetic application.

The UV ray can be divided into three parts by wavelength as UV-A (320–400 nm), UV-B (280–320 nm) and UV-C (200–280 nm). Since UV-C and most of UV-B are absorbed by ozone layer in the upper atmosphere, the UV ray in the sunlight which reaches on the ground is mainly UV-A (90–99%), and UV-B is also contained slightly (1–10%). Therefore, the UV shielding materials are expected to absorb UV-A as well as UV-B. In order to evaluate UV shielding ability of non-coated and silica-coated CaO-doped ceria/potassium lithium titanate nanocomposite, the UV–Vis transmittance spectra of the samples were determined and the results are shown in Fig. 11. The transparencies in the visible light region of non-coated and silica-coated CaO-doped ceria/potassium lithium titanate samples were slightly lower than that of CaO-doped ceria sample which may be due to scattering of visible light rays by large plate-like potassium lithium titanate particles. On the other hand, the UV shielding properties CaO-doped ceria/potassium lithium titanate were superior to that of CaO-doped ceria sample probably due to better distribution of CaO-doped ceria after coupling with regular shape and larger particles size potassium lithium titanate materials. In addition potassium lithium

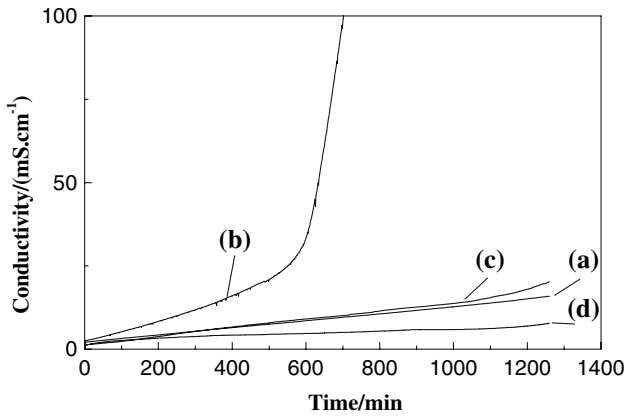

Fig. 9 Evaluation of the oxidation catalytic activity by Rancimat method at 120 °C: (**a**) blank, (**b**) CaO-doped ceria (**c**) CaO-doped ceria/potassium lithium titanate, CaO-doped ceria/potassium lithium titanate coated with 5 wt% silica for (**d**) 180 min

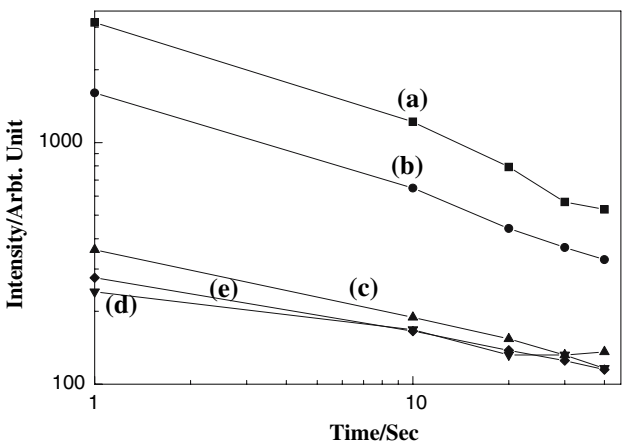

Fig. 10 Chemiluminescence caused by singlet oxygen determined by irradiating the sample powder with UV rays at room temperature, (**a**) TiO_2, (**b**) ZnO, (**c**) undoped CeO_2, and (**d**) CaO-doped ceria, CaO-doped ceria/potassium lithium titanate coated with 5 wt% silica for (**e**) 180 min

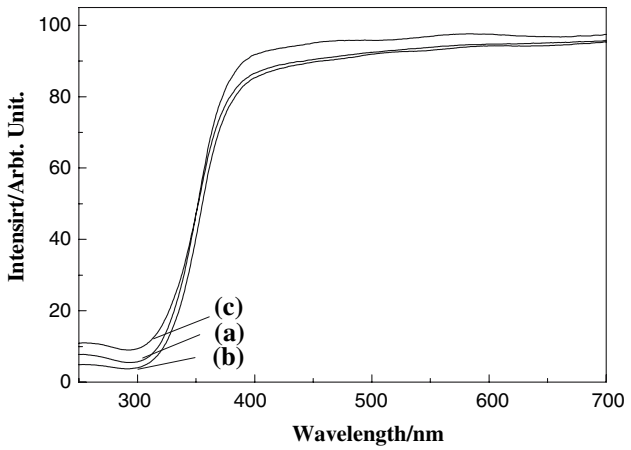

Fig. 11 UV–Vis transmittance spectra of thin films of (**b**) CaO-doped ceria, (**a**) calcia-doped ceria/plate-like potassium lithium titanate, (**c**) 5 wt% silica-coated CaO-doped ceria/potassium lithium titanate for 180 min

titanate is n-type semiconductor possessing UV-shielding ability. These results turn light on the importance of coupling of CaO-doped ceria nanoparticles with plate-like materials to improve its UV-rays blocking properties.

Conclusions

UV shielding properties of CaO-doped ceria was enhanced by coupling with plate-like potassium lithium titanate particles. CaO-doped ceria/potassium lithium titanate shows the superior UV-shielding properties compared with that of CaO-doped ceria despite the decrease of cerium content. Characterization of non-coated and silica-coated CaO-doped ceria/plate-like potassium lithium titanate by SEM, TEM, and FTIR indicates the coverage of plate-like potassium lithium titanate surfaces with CaO-doped ceria nanoparticles and development of silica shell on CaO-doped ceria surface. The catalytic ability of CaO-doped ceria/plate-like potassium lithium titanate nanocomposite for air oxidation of castor oil was lower than that of CaO-doped ceria nanoparticles.

Acknowledgements This research was carried out as one of the projects in MSTEC Research Center at IMRAM, Tohoku University and partially supported by the Ministry of Education, Culture, Sports, Science and Technology, a Grant-in-Aid for the Scientific Research of Priority Areas (Panoscopic Assembling and High Ordered Functions for Rare Earth Materials).

References

1. Sato T, Katakura T, Yin S, Fujimoto T, Yabe S (2004) Soild State Ionics 172:377
2. Ryabchikov DI, ryuabukin VA (1970) In: Analytical chemistry of Yttrium and the lanthanide elements; ed. Ann Arbor, Ann Arbor-Humphrey Sci., Michigan, Chapter 3, 50
3. Chen P, Chen I (1993) J Am Ceram Soc 76:1577
4. Zhou Y, Philips R, Switzer J (1995) J Am Ceram Soc 78:981
5. Hirano M, Kato E (1996) J Am Ceram Soc 79:777
6. Masui T, Fujiwara K, Machida K, Sakata T, Mori H, Adachi G (1997) Chem Mater 9:2197
7. Masui T, Machida K, Sakata T, Mori H, Adachi G (1997) J Alloys Compd 309:127
8. Yu X, Li F, Ye X, Xin X, Xue Z (2000) J Am Ceram Soc 83:964
9. Yabe S, Yamashita M, Momose S, Tahira K, Yoshida S, Li R, Yin S, Sato T (2001) Inter J Inorg Mater 3:1003
10. Yabe S, Sato T (2003) J Sol Stat Chem 171:7
11. IIer RK U.S. Patent No. 2,885,336,1959
12. Philipse AP, Van Bruggen MPB, Pathmamanoharan C (1994) Langmuir 10:92
13. Liz-Marzán LM, Philipse AP (1995) J Colloid Interface Sci 176:459
14. Liz-Marzán LM, Giersig M, Mulvaney P (1996) Langmuir 12:4329
15. Ung T, Liz-Marzán LM, Mulvaney P (1998) Langmuir 14:370
16. Adair JH, Li T, Havey K, Moon J, Mecholsky A, Morrone A, Talham DR, Ludwig MH, Wang L (1998) Mater Sci Eng R 23:139
17. Liu Q, Xu Z, Finch JA, Egerton R (1998) Chem Mater 10:3936
18. Yabe S, Yamashita M, Momose S, Yoshida S, Hasegawa K, Yin S, Sato T (2001) J Soc Inorg Mater Jpn 8:428
19. Kobayashi Y, Misawa K, Kobayashi M, Takeda M, Konno M, Satake M, Kawazoe Y, Ohuchi N, Kasuya A (2004) Colloid and Surf A: Physicochem Eng Aspects 242:47
20. Kobayashi Y, Misawa K, Takeda M, Kobayashi M, Satake M, Kawazoe Y, Ohuchi N, Kasuya A, Konno M (2004) Colloid Surf A: Physicochem Eng Aspects 251:197
21. Stöber W, Fink A, Bohn E (1968) J Colloid Interface Sci 26:62
22. El-Toni AM, Yin S, Hayasaka Y, Sato Tsugio (2005) J Mater Chem 15:1293
23. Feng Q, Hirasawa M, Yanagisawa K (2001) Chem Mater 13:290
24. Sasaki T, Kooli F, Iida M, Michiue Y, Takenouchi S, Yajima Y, Izumi F, Chakoumakos BC, Watanabe M (1998) Chem Mater 10:4123
25. Yabe S, Momose S (1998) J Soc Cosmat Chem Jpn 32:372
26. Kanofsky JR (1989) Chem-Biol Interact 70:1